photonics

MDPI

Article

Polarization-Dependent Absorption and Transmission Metasurfaces for Linearly and Circularly Polarized Light in Terahertz Band

Bowei Yang [1], Mingzhao Ouyang [1,2,3], Hang Ren [1,2,3], Jinshuang Wu [1], Yixin Zhang [4] and Yuegang Fu [1,2,3,*]

[1] School of Optoelectronic Engineering, Changchun University of Science and Technology, Changchun 130022, China
[2] Key Laboratory of Optoelectronic Measurement and Optical Information Transmission Technology of Ministry of Education, Changchun University of Science and Technology, Changchun 130022, China
[3] Key Laboratory of Advanced Optical System Design and Manufacturing Technology of the Universities of Jilin Province, Changchun 130022, China
[4] Changchun Jingyi Optoelectronic Technology Co., Ltd., Changchun 130012, China
* Correspondence: fuyg@cust.edu.cn

Abstract: Polarization detection is an important part of many polarization applications such as polarization imaging, wireless communication, and circular dichroism spectroscopy. In this paper, two polarization-dependent terahertz wave absorption and transmission metasurface for linearly and circularly polarized light are proposed and proved by numerical simulations. Polarization filtering and polarization absorption are integrated on a single cell, and the orthogonal polarization component is transmitted and absorbed, respectively. The linearly polarization-dependent transmission and absorption structure can obtain a transmission extinction ratio of 11.5 dB and an absorption extinction ratio of over 270 dB at 3 THz. Moreover, the circularly polarization-dependent structure can obtain a transmission extinction ratio of 8.1 dB and an absorption extinction ratio of 4.66 dB at 2.8 THz. Our design facilitates the acquisition of full Stokes parameters and the high-resolution imaging.

Keywords: terahertz; polarization-dependent; filtering; absorption

Citation: Yang, B.; Ouyang, M.; Ren, H.; Wu, J.; Zhang, Y.; Fu, Y. Polarization-Dependent Absorption and Transmission Metasurfaces for Linearly and Circularly Polarized Light in Terahertz Band. *Photonics* **2023**, *10*, 100. https://doi.org/10.3390/photonics10020100

Received: 7 December 2022
Revised: 28 December 2022
Accepted: 4 January 2023
Published: 17 January 2023

1. Introduction

Terahertz technology has been widely used in nondestructive testing [1,2], high-speed communication [3,4], and astronomical observations [5,6]. Terahertz metasurface absorbers can be used for sensors [7–10] and communication receivers [11] and have been extensively investigated. Most studies design metasurface shapes to be completely symmetrical in order to maximize the absorption of the incident spectrum, however these structures could result in the metasurface polarization insensitive [12–15]. Asymmetric structure can cause different electromagnetic responses in different directions of the metasurface. There have been studies to realize linear polarization-dependent devices through asymmetric structure [16–18]. Circular polarization dependence can be also achieved by chiral patterns [19–22]. However, these studies can only perform real-time detection of one polarization state at the same frequency in a single cell. If the Stokes vector method is used to characterize the polarization information, six units are needed to detect the intensity information of linearly polarized light in four directions and circularly polarized light in two rotation directions, respectively [23,24]. Multiple polarization elements lead to loss of spatial resolution in the detection plane as well as positional errors, which is not conducive to the development of high-resolution polarization imaging devices.

In this paper, polarization-dependent transmission and absorption metasurface for linearly and circularly polarized light are proposed. Filtering and absorption are integrated in the same cell; one polarization component is absorbed, and the other is transmitted at the same time. Hence, a pair of orthogonal linearly polarized light or circularly polarized

light with opposite rotational directions can be detected simultaneously in a single incident light beam. Only three groups of metasurfaces are required to obtain the complete Stokes parameters, and position errors can be effectively reduced. These results reveal that our design can facilitate the development of high-resolution polarization imaging and detection.

2. Results and Discussion

2.1. Polarization Dependent Transmission and Absorption Structure for Linearly Polarized Light

The polarization dependent absorption structure is first designed as the basic structure. Figure 1 shows the line polarization dependent absorption structure. The metasurface absorber is designed as the classic sandwich structure. The top layer is a rectangular patch of material Au. The length of the rectangle determines the absorption frequency of the metasurface. The middle layer is epoxy resin, which has a relative dielectric constant of $\varepsilon_r = 1.4$ [17]. The bottom layer is made of Au. The thickness of both layers of Au is 100 nm. Since the skinning depth in the terahertz band is less than 100 nm, all incident waves are reflected or absorbed. The expression for the absorption rate can be simplified as $A = 1 - R$. The commercial software FDTD solution is used for the simulation analysis of the designed metasurface. The TM wave is set parallel to the long side of the rectangle and the TE wave is parallel to the short side.

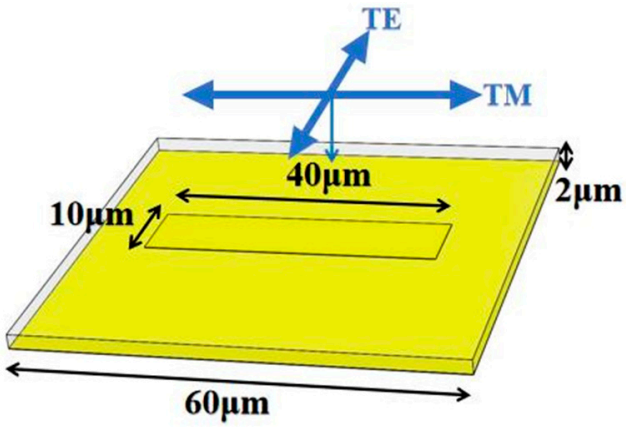

Figure 1. Schematic diagram of the composite metasurface structure. The rectangular structure is 40 μm long and 10 μm wide. The period of the structure is 60 μm. The thickness of the medium is 2 μm.

Firstly, the influence of structural parameters on performance is simulated. Here, the cycle of the structure is fixed at 60 μm. The thickness of the dielectric layer is fixed at 2μ m. As shown in Figure 2a, the length of the structure is inversely proportional to the absorption frequency. The length of the structure only affects the response frequency and does not affect the absorption performance of the structure. The reflectivity at the five response frequencies in Figure 2a is less than 2%, and the absorptivity exceeds 98%. In addition, the influence of structure width on the structure is simulated. As shown in Figure 2b, the broadening of the structure will result in a slight decrease in the response frequency and absorptivity, and a slight increase in the reflectivity. This may be caused by the change of relative area of capacitance between upper and lower layers. It is considered that the transmission function will be introduced for TE light subsequently, so the width of the resonator should be small enough to avoid causing resonance in the y-direction of the target wave band, which will cause the absorption or reflection of TE light to reduce the transmittance.

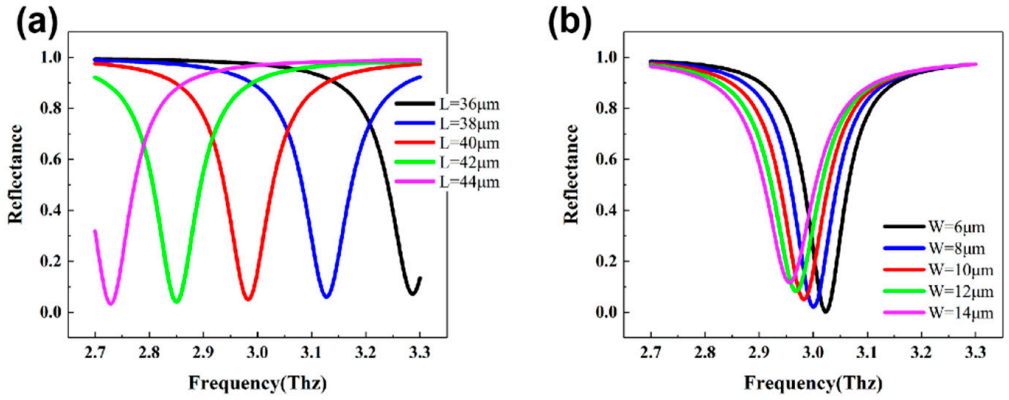

Figure 2. (**a**) The effect of resonant metal length on structure reflectivity. (**b**) The effect of resonant metal width on structure reflectivity.

The absorption rate of the absorber is mainly affected by the thickness of the dielectric layer. Figure 3a shows the effect of different dielectric layer thicknesses on structural reflectance. Here, the length of the upper resonator is fixed at 40 × 10 μm, and the period is fixed at 60 μm. As the thickness of the medium increases, the resonant frequency decreases. When the thickness of the medium is 2 μm, the lowest reflectivity and the best absorptivity can be obtained. Figure 3b shows the effect of the period on the reflectance. The length of the upper resonator is fixed at 40 × 10 μm, and the thickness of the dielectric layer is 2 μm. When the period is between 60–80 μm, there is almost no reflected light, and the structure has strong absorption. When the period increased to 90 μm, the reflectivity began to increase slightly.

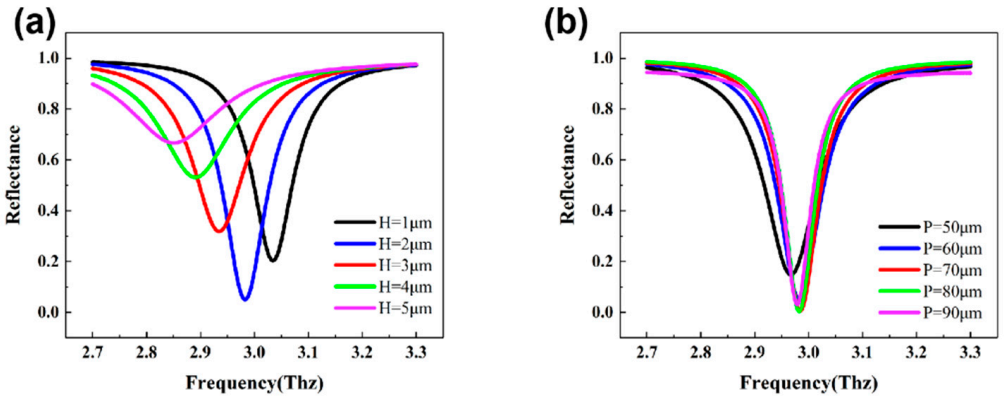

Figure 3. (**a**) The effect of absorber medium layer thickness on structure reflectivity. (**b**) The effect of the period on structure reflectivity.

From the above results, it can be concluded that the resonant frequency is mainly affected by the length of the resonator, while the absorption is mainly affected by the thickness of the dielectric layer. By adjusting the parameters of the structure, the ideal absorption frequency and absorptivity can be obtained. In order to reveal the physical mechanism of structural absorption, parameters with good absorption (as shown in Figure 1) are selected for simulation. Figure 4a shows the spectral response of the metasurface. The TM wave has a strong absorption peak at 3.03 THz with an absorption of over 97%. The TE wave has a reflection of over 99% at the entire simulated frequency and cannot trigger the absorption mode and the absorption rate is less than 1%. The electric and magnetic fields at 3.03 THz are simulated. When a TM wave is incident, the incident electric field couples with the rectangle and gathers at both ends of the rectangle. Incident waves excite the localized surface plasmon. A strong magnetic field exists in the medium below the rectangle and

induces an absorption mode. TE waves cannot excite resonance and magnetic fields. The incident wave is reflected completely by the bottom metal.

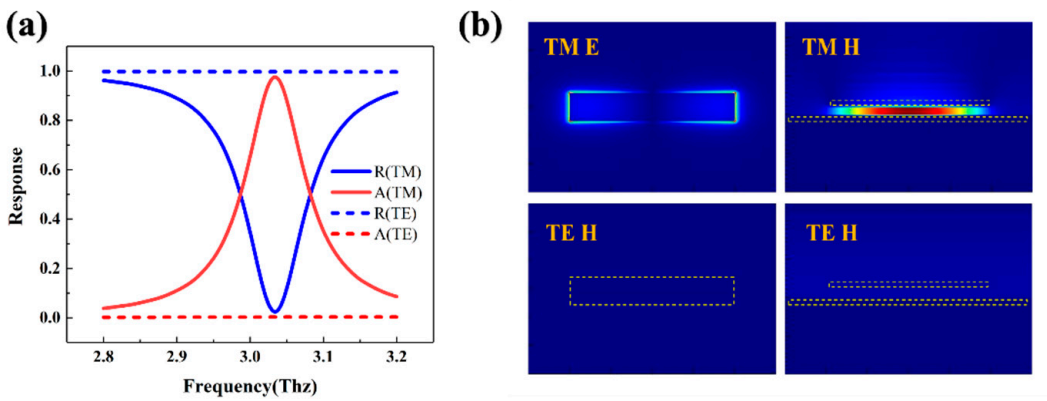

Figure 4. (**a**) Response spectrum (absorption and reflectance) of TM and TE polarized light. (**b**) Electric and magnetic field distribution at the absorption peak (electric field at the top structure in the xy plane and magnetic field in the xz cross section).

Further, transmission mode is added to the metasurface. As shown in Figure 5a, the bottom metal of the base model is replaced by a metal wire grid. The metal wire grid has a line polarization filtering effect. Due to software limitations, only one simulation region can be built in the simulation, so the period of the grid can only be the same as the period of the resonator or reduced by an integer multiple. The transmittance of TM and TE waves at 0.5 duty cycle is simulated. As shown in Figure 5b, when the period is 15 µm, the TE wave has the highest transmittance, and the polarization differentiation characteristic of the grid is the best. The effect of line width on transmittance is simulated. As shown in Figure 5c,d, the larger the line width, the lower the transmittance, but the transmission extinction ratio (Defined as T_{TE}/T_{TM}) increases. High extinction ratio means that the structure has a good ability to distinguish polarization state, and high transmittance means that the structure has less loss to the incident wave. In order to satisfy both high transmittance and extinction ratio, 8µm was selected as the line width. The transmittance of TE waves exceeds 96%, while the transmittance of TM waves is less than 1%. The extinction ratio exceeds 94 dB in the simulated wavelength band. As shown in Figure 5c, TM waves cannot induce surface plasmon. Therefore, TM waves cannot be transmitted. Additionally, the TE wave can induce the surface plasma, resulting in a high zero-order transmission generation [25].

The absorptivity of the metasurface is calculated by $A = 1 - R - T$. Figure 6a shows the spectral response of the composite structure. The TM wave has a significant absorption of more than 85% near 3 THz, while the transmittance is less than 8.3%. The TM wave has a slight increase in transmittance near 3 THz. This is due to the excitation of the surface plasma by the rectangular structure and the enhanced electric field in the lower layer, resulting in a slight increase in transmittance. The transmittance of TE waves exceeds 95% and the absorption rate is less than 1%. Due to the extremely low TE absorption, the absorption extinction ratio (Defined as A_{TM}/A_{TE}) exceeds 270 dB within the whole simulation frequency, while the transmission extinction ratio (Defined as T_{TE}/T_{TM}) can reach a maximum of 11.5 dB. The slight decrease in absorption frequency may be due to the change in capacitance caused by the reduction in the relative area of the upper and lower layers. Figure 6b shows the electric and magnetic fields of the composite structure. The transmitting and absorbing structure has similar electric and magnetic fields to the basic structure. Therefore, the absorption mode of the metasurface remains valid. Although the absorption efficiency and extinction ratio are slightly decreased due to the slight increase in transmittance of TM waves, both transmittance and absorption extinction ratios can be obtained in a single cell.

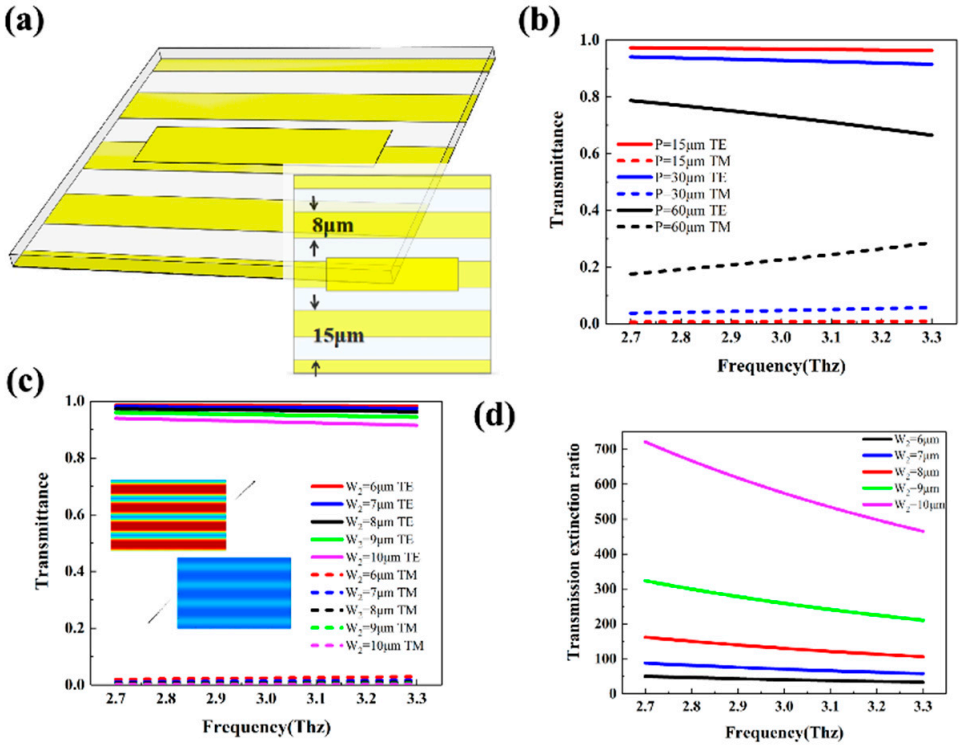

Figure 5. (**a**) Schematic diagram of the composite supersurface structure. The wire grid has a line width of 8 μm and a period of 15 μm. (**b**) The effect of grid period on transmissivity. (**c**) The effect of grid width on transmissivity. (**d**) The effect of grid width on extinction ratio.

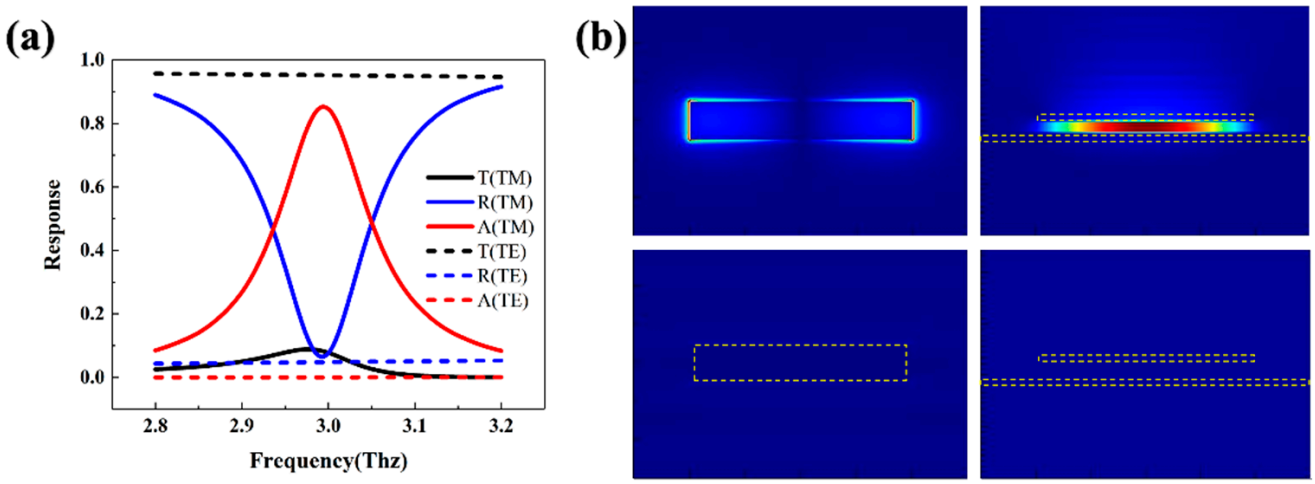

Figure 6. (**a**) Response spectrum (absorption, reflectivity, and transmission) of TM and TE polarized light. (**b**) Electric and magnetic field distribution at the absorption and transmission peaks (electric field at the top structure in the xy plane and magnetic field in the xz cross section).

The dependence of the transmission and absorption ratios at 2.976 THz on the polarization angle (from 0° to 90°) of incident light is simulated. As shown in Figure 7, the reflectance is always below 8%. As the polarization angle increases from 0° to 90°, there is a linear decline and increase in the absorbance and transmittance, respectively. The absorption reaches a maximum of 84% at a polarization angle of 0°, and the transmittance reaches a maximum of 95% at a polarization angle of 90°. Hence, our design can be used for polarization angle measurement of incident light. It can also be used for the measurement of 0° and 90° polarized light intensity.

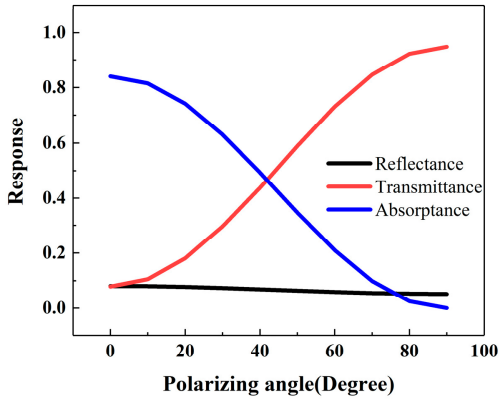

Figure 7. The effect of incident light polarization angle on transmission and reflection ratios.

2.2. Polarization-Dependent Transmission and Absorption Structure for Circularly Polarized Light

Firstly, the polarization dependent absorption structure for circularly polarized light is designed as the basic structure. The chiral structure can effectively distinguish the circularly polarized light, hence a tilted rectangle is added to break the mirror symmetry of the structure. The chiral structure is shown in Figure 8a. Previous research shows that the period of structure is 60–80 μm and has good absorption. Since a resonant metal is added and rotated, in order to ensure the spacing between structures, the period of the structure is increased to 80 μm. In the simulation settings, the length and width of the other resonant metal remain unchanged. However, FDTD has errors in mesh segmentation of inclined objects, so the actual length is close to 41 × 11 μm (The mesh precision is 0.5 um × 0.5 um × 0.5 um). The influence of the thickness of the dielectric layer and the rotation angle of the resonant metal on the absorption performance of the chiral structure is simulated. Figure 8b shows the influence of different media layer thickness on the reflectivity of the chiral structure. As the thickness of the medium increases, the resonance frequency decreases. The absorption peak of chiral structure occurs when the medium thickness is 5 μm, the reflectivity is the lowest, and most of the incident light is absorbed. Figure 8c shows the effect of the resonant metal rotation angle on the reflectivity of the chiral structure. The results show that the rotation angle between 20° and 30° has low reflectivity and strong absorption.

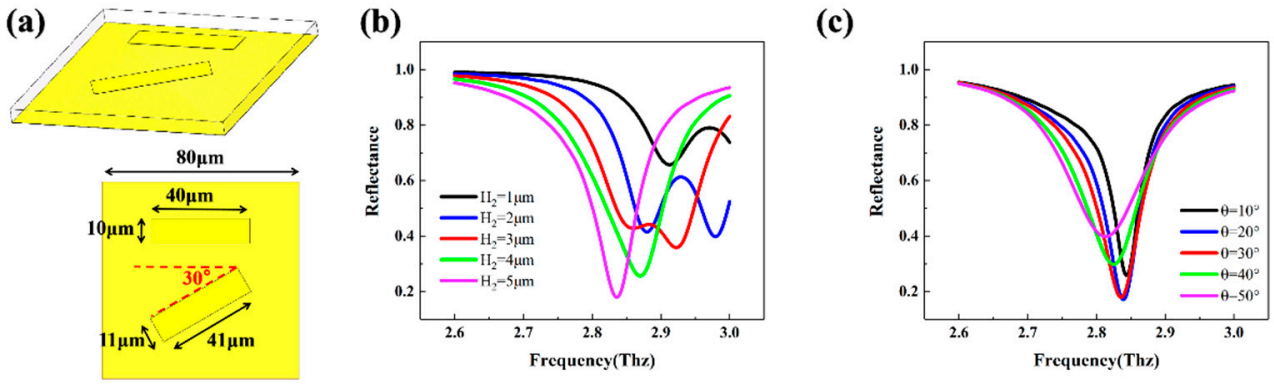

Figure 8. (**a**) Schematic diagram of the chiral structure. The tilted rectangle is 41 μm long, and 11 μm wide. The optimized thickness of the medium is 5 μm. (**b**) The effect of the thickness and length of the dielectric layer on the reflectivity of the chiral structure. (**c**) The effect of resonance metal rotation angle on the reflectivity of chiral structures.

Figure 9a shows the spectral response of the chiral structure. The left-handed polarized light shows a clear absorption peak near 2.88 THz. The maximum absorption exceeds

85%. At the same frequency, the absorption of right-handed polarized light is less than 15%. Figure 9b shows the electric and magnetic field response of the metasurface. The left-handed polarized light can produce dipole resonance at the two rectangular ends and the localized surface plasma is excited. The presence of a strong magnetic field in the dielectric layer beneath the structure induces absorption mode. The surface plasma can also be excited by the incident right-handed polarized light. However, the electric and magnetic fields are less intense. The right-handed polarized light is also partially absorbed, and the absorption rate is lower. The circular polarization extinction ratio (defined as T_{Left}/T_{Right}) can reach a maximum of 5.6 dB.

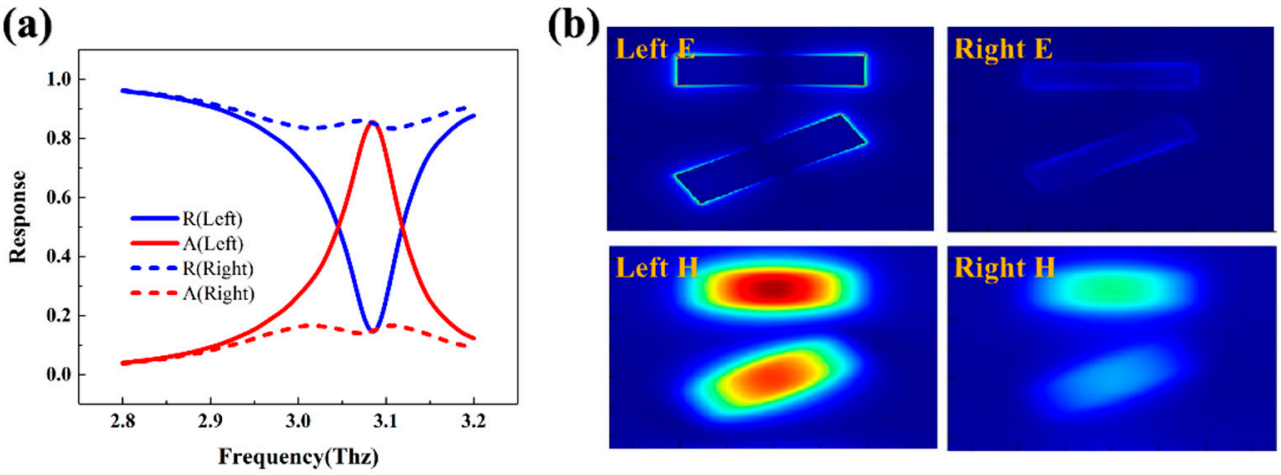

Figure 9. (**a**) Response spectrum (absorption and reflectance) of left and right -handed polarized light. (**b**) Electric and magnetic field distribution at the absorption peak (electric field at the top structure in the xy plane, and magnetic field in the middle xy section of the medium).

On this basis, the polarization-dependent transmission and absorption structure for circularly polarized light is proposed. The parameters of the structure are shown in Figure 10a. The chiral hole is added to the bottom metal film. The shape of the hole is similar to the top metal, which results in better coupling of the surface plasma. Figure 10b shows the spectral response of the rectangular holes in the metal film. It can be found that the single-layer hole structure has no asymmetric transmission characteristics. The peak transmittance is close to 50%. There is a slight dipole resonance at the peak, which induces transmission. Figure 10c shows the spectral response of the metasurface. The absorption of left-handed polarized light reaches the maximum of 70%, and the transmissivity of right-handed polarized light reaches the maximum of 61% at 2.8 THz. The absorption extinction ratio (Defined as T_{Left}/T_{Right}) and transmission extinction ratio (Defined as T_{Right}/T_{Left}) reach 4.66 dB and 8.1 dB, respectively. Although a great extinction ratio cannot be obtained, the structure can still effectively distinguish the handedness of circularly polarized light. To investigate the physical mechanisms of absorption and transmission, the electric field of the top and bottom layers and the magnetic field of the middle layer are simulated. The top electric field and the internal magnetic field are close to the basic structure when the left-handed polarized light is incident. Therefore, the structure can still obtain a high absorbance. The metal edge at the bottom also produces a weaker resonance, so the structure has a slight transmission. Additionally, when right-handed polarized light is incident, the magnetic field is weak and only slight absorption is obtained. Additionally, the resonance at the bottom is higher than the single-layer hole structure, which can obtain a higher transmission. Overall, the better extinction ratio of linearly polarization-dependent structures can be attributed to two main reasons. First, chiral structure has a relatively weak differentiation ability, resulting in a poorer absorption extinction ratio. The second is that the bottom structure of the linearly polarized transmission structure has extremely strong

asymmetric transmission, which allows for an ultra-high transmission extinction ratio. In contrast, the bottom of the circularly polarized transmission structure does not have asymmetric transmission, and the transmission difference is caused by the combined effect of local surface excitations absorption and enhanced lower electric field. Compared to the basic structure, the transmission and absorption structure reduce a little of the absorption extinction ratio and add the transmission mode. This allows us to obtain two polarization information at the same time for the same frequency in one beam of light.

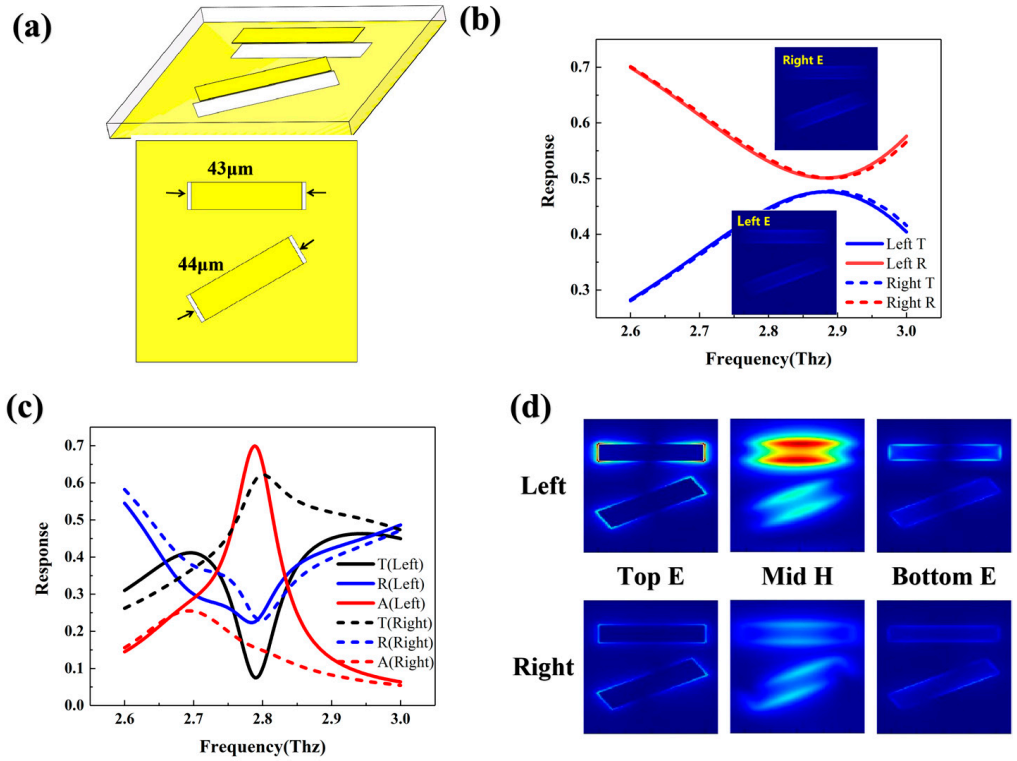

Figure 10. (**a**) Schematic diagram of the chiral composite structure. The dimensions of the top structure and medium are the same as the basic structure. The lengths of the rectangular holes are 43 μm and 44 μm. (**b**) The transmission efficiency and the corresponding electric field of the rectangular hole structure for left and right-handed polarized light. (**c**) Response spectrum (absorption, reflectivity, and transmission) of left and right-handed polarized light. (**d**) Electric and magnetic field distribution at the absorption and transmission peaks (electric field at the top and bottom structure in the xy plane, and magnetic field in the middle xy section of the medium).

The structure we designed can be used for the acquisition of Stokes parameters. The complete Stokes detection requires the acquisition of six light intensity parameters, which are the intensity of linearly polarized light at 0°, 45°, 90°, and 135°, and the intensity of two types of circularly polarized light. Figure 11 shows the full Stokes parameter detection structure. The function of Unit A and Unit C has been verified by the studies above. Unit A absorbs linearly polarized light of 0° and transmits linearly polarized light of 90°. Unit C absorbs right-handed polarized light and transmits left-handed polarized light. Unit B is created by rotating unit A by 45 degrees without changing any structural parameters. Therefore, Unit B absorbs linearly polarized light of 45° and transmits linearly polarized light of 135°. This allows 0° and 45° linearly polarized light and right-handed polarized light to be absorbed by metamaterials, and their intensity can be measured by absorption detection elements. The 90° and 135° linearly polarized light and left-handed polarized light will be transmitted, and can be further absorbed and detected by the lower layer detector. The structure we designed can play the role of polarization filtering and absorption in the detection system. Full Stokes parameter can be detected in three cells,

while the conventional split-focus plane approach requires six cells [26]. In comparison, our design has a smaller spatial position error, which is conducive to the development of high-resolution devices.

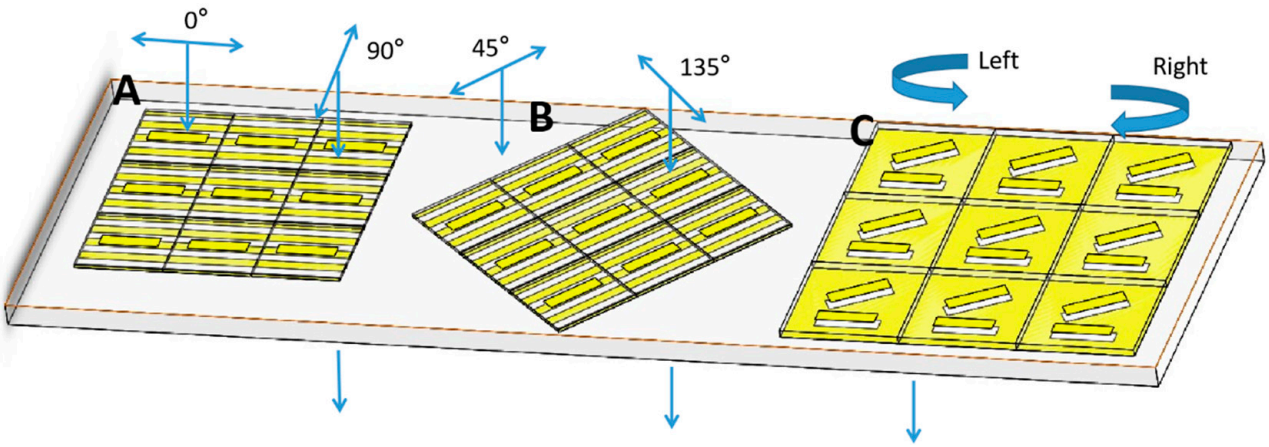

Figure 11. Full Stokes parameter detection structure.

3. Conclusions

In conclusion, two polarization-dependent transmission and absorption metasurfaces are proposed. The performance of the structure is verified by numerical simulations using the finite-difference time-domain method. The results show that the linearly polarization-dependent transmission and absorption structure can obtain a transmission extinction ratio of 11.5 dB and an absorption extinction ratio of over 270 dB at 3 THz. Meanwhile, the circularly polarization-dependent structure can obtain a transmission extinction ratio of 8.1 dB and an absorption extinction ratio of 4.66 dB at 2.8 THz. Compared to previous studies, the structure allows two types of polarization information to be obtained simultaneously in one beam of light. Our findings are helpful for the development of high-resolution polarization imaging and detection.

Author Contributions: Conceptualization, B.Y. and Y.F.; Data curation, B.Y.; Formal analysis, B.Y.; Funding acquisition, Y.Z. and Y.F.; Investigation, B.Y.; Methodology, B.Y.; Project administration, B.Y. and M.O.; Resources, B.Y.; Software, B.Y. and Y.Z.; Supervision, B.Y.; Validation, B.Y., J.W. and Y.F.; Visualization, B.Y.; Writing—original draft, B.Y.; Writing—review and editing, M.O. and H.R. All authors have read and agreed to the published version of the manuscript.

Funding: This study received funding from Science and technology research project of Education Department of Jilin Province (JJKH20210814KJ), National Natural Science Foundation of China (61705018), 111 Project of China (D21009, D17017).

Institutional Review Board Statement: Not applicable.

Informed Consent Statement: Not applicable.

Data Availability Statement: The data presented in this study are available on request from the corresponding author. The data are not publicly available due to further study.

Conflicts of Interest: The authors declare no conflict of interest.

References

1. Zhong, S. Progress in terahertz nondestructive testing: A review. *Front. Mech. Eng.* **2019**, *14*, 273–281. [CrossRef]
2. Amenabar, I.; Lopez, F.; Mendikute, A. In introductory review to THz non-destructive testing of composite mater. *J. Infrared Millim. Terahertz Waves* **2013**, *34*, 152–169. [CrossRef]
3. Goyal, R. Vishwakarma D K. Design of a graphene-based patch antenna on glass substrate for high-speed terahertz communications. *Microw. Opt. Technol. Lett.* **2018**, *60*, 1594–1600. [CrossRef]

4. Jia, S.; Wang, S.; Liu, K.; Pang, X.; Zhang, H.; Jin, X.; Zheng, S.; Chi, H.; Zhang, X.; Yu, X. A unified system with integrated generation of high-speed communication and high-resolution sensing signals based on THz photonics. *J. Light. Technol.* **2018**, *36*, 4549–4556. [CrossRef]
5. Withington, S. Terahertz astronomical telescopes and instrumentation. Philosophical Transactions of the Royal Society of London. *Ser. A Math. Phys. Eng. Sci.* **2004**, *362*, 395–402.
6. Kulesa, C. Terahertz spectroscopy for astronomy: From comets to cosmology. *IEEE Trans. Terahertz Sci. Technol.* **2011**, *1*, 232–240. [CrossRef]
7. Shangguan, Q.; Chen, Z.; Yang, H.; Cheng, S.; Yang, W.; Yi, Z.; Wu, X.; Wang, S.; Yi, Y.; Wu, P. Design of ultra-narrow band graphene refractive index sensor. *Sensors* **2022**, *22*, 6483. [CrossRef]
8. Wang, X.; Lin, J.; Yan, Z.; Yi, Z.; Yu, J.; Zhang, W.; Qin, F.; Wu, X.; Zhang, J.; Wu, P. Tunable high-sensitivity sensing detector based on Bulk Dirac semimetal. *RSC Adv.* **2022**, *12*, 32583–32591. [CrossRef]
9. Escorcia, I.; Grant, J.; Gough, J.; Cumming, D.R.S. Uncooled CMOS terahertz imager using a metamaterial absorber and pn diode. *Opt. Lett.* **2016**, *41*, 3261–3264. [CrossRef]
10. Carranza, I.E.; Grant, J.P.; Gough, J.; Cumming, D. Terahertz metamaterial absorbers implemented in CMOS technology for imaging applications: Scaling to large format focal plane arrays. *IEEE J. Sel. Top. Quantum Electron.* **2016**, *23*, 2630307.
11. Jornet, J.M.; Akyildiz, I.F. Graphene-based plasmonic nano-antenna for terahertz band communication in nanonetworks. *IEEE J. Sel. Areas Commun.* **2013**, *31*, 685–694. [CrossRef]
12. Pan, W.; Shen, T.; Ma, Y.; Zhang, Z.; Yang, H.; Wang, X.; Zhang, X.; Li, Y.; Yang, L. Dual-band and polarization-independent metamaterial terahertz narrowband absorber. *Appl. Opt.* **2021**, *60*, 2235–2241. [CrossRef]
13. Zheng, Z.; Zheng, Y.; Luo, Y.; Yi, Z.; Zhang, J.; Liu, Z.; Yang, W.; Yu, Y.; Wu, X.; Wu, P. A switchable terahertz device combining ultra-wideband absorption and ultra-wideband complete reflection. *Phys. Chem. Chem. Phys.* **2022**, *24*, 2527–2533. [CrossRef] [PubMed]
14. Ning, R.; Bao, J.; Jiao, Z.; Xu, Y. Omnidirectional polarization-insensitive tunable absorption in graphene metamaterial of nanodisk structure. *J. Appl. Phys.* **2015**, *118*, 203101. [CrossRef]
15. Chen, H.; Chen, Z.; Yang, H.; Wen, L.; Yi, Z.; Zhou, Z.; Dai, B.; Zhang, J.; Wu, X.; Wu, P. Multi-mode surface plasmon resonance absorber based on dart-type single-layer graphene. *RSC Adv.* **2022**, *12*, 7821–7829. [CrossRef] [PubMed]
16. Hokmabadi, M.P.; Wilbert, D.S.; Kung, P.; Kim, S.M. Polarization-dependent, frequency-selective THz stereometamaterial perfect absorber. *Phys. Rev. Appl.* **2014**, *1*, 044003. [CrossRef]
17. Hu, F.; Zou, T.; Quan, B.; Xu, X.; Bo, S.; Chen, T.; Wang, L.; Gu, C.; Li, J. Polarization-dependent terahertz metamaterial absorber with high absorption in two orthogonal directions. *Opt. Commun.* **2014**, *332*, 321–326. [CrossRef]
18. Yu, H.; Meng, D.; Liang, Z.; Xu, H.; Qin, Z.; Su, X.; Smith, D.R.; Liu, Y. Polarization-dependent broadband absorber based on composite metamaterials in the long-wavelength infrared range. *Opt. Express* **2021**, *29*, 36111–36120. [CrossRef]
19. Ouyang, L.; Wang, W.; Rosenmann, D.; Czaplewski, D.A.; Gao, J.; Yang, X. Near-infrared chiral plasmonic metasurface absorbers. *Opt. Express* **2018**, *26*, 31484–31489. [CrossRef]
20. Mahmud, M.S.; Rosenmann, D.; Czaplewski, D.A.; Gao, J.; Yang, X. Chiral plasmonic metasurface absorbers in the mid-infrared wavelength range. *Opt. Lett.* **2020**, *45*, 5372–5375. [CrossRef]
21. Tang, H.; Rosenmann, D.; Czaplewski, D.A.; Yang, X.; Gao, J. Dual-band selective circular dichroism in mid-infrared chiral metasurfaces. *Opt. Express* **2022**, *30*, 20063–20075. [CrossRef] [PubMed]
22. Tang, B.; Li, Z.; Palacios, E.; Liu, Z.; Butun, S.; Aydin, K. Chiral-selective plasmonic metasurface absorbers operating at visible frequencies. *IEEE Photonics Technol. Lett.* **2017**, *29*, 295–298. [CrossRef]
23. Wu, P.C.; Chen, J.W.; Yin, C.W.; Lai, Y.C.; Chung, T.L.; Liao, C.Y.; Chen, B.H.; Lee, K.-W.; Chuang, C.-J.; Wang, C.-M.; et al. Visible metasurfaces for on-chip polarimetry. *ACS Photonics* **2017**, *5*, 2568–2573. [CrossRef]
24. Arbabi, E.; Kamali, S.M.; Arbabi, A.; Faraon, A. Full-Stokes imaging polarimetry using dielectric metasurfaces. *ACS Photonics* **2018**, *5*, 3132–3140. [CrossRef]
25. Brand, G.F. The strip grating as a circular polarizer. *Am. J. Phys.* **2003**, *71*, 452–456. [CrossRef]
26. Basiri, A.; Chen, X.; Bai, J.; Amrollahi, P.; Carpenter, J.; Holman, Z.; Wang, C.; Yao, Y. Nature-inspired chiral metasurfaces for circular polarization detection and full-Stokes polarimetric measurements. *Light Sci. Appl.* **2019**, *8*, 78. [CrossRef]